AIAA JOURNAL
Vol. 32, No. 2, February 1994

Simulation of Transition with a Two-Equation Turbulence Model

David C. Wilcox*
DCW Industries, Inc., La Cañada, California 91011

This paper demonstrates how well the k-ω turbulence model describes the nonlinear growth of flow instabilities from laminar flow into the turbulent flow regime. Viscous modifications are proposed for the k-ω model that yield close agreement with measurements and with direct numerical simulation results for channel and pipe flow. These modifications permit prediction of subtle sublayer details such as maximum dissipation at the surface, $k \sim y^2$ as $y \to 0$, and the sharp peak value of k near the surface. With two transition specific closure coefficients, the model equations yield a realistic description of a transitional incompressible flat-plate boundary layer. A new concept known as the numerical roughness strip is introduced that permits triggering transition at a desired location. A series of transitional boundary-layer applications, including effects of surface heat transfer, pressure gradient and freestream Mach number, verify that the numerical roughness strip is very effective in triggering transition and that flow in the transitional region is realistically described.

I. Introduction

THERE has been renewed interest in development of methods for predicting boundary-layer transition. Current interest in vehicles such as the National Aerospace Plane (NASP), for example, provides the impetus for developing accurate transition prediction tools. Furthermore, because hypersonic boundary layers rarely achieve momentum-thickness Reynolds numbers large enough to sustain fully developed turbulence, even the post-transition region generally exhibits nontrivial viscous effects. Consequently, accurate low-Reynolds-number turbulence models are also needed.

The standard approach is to view development of a transition model and a low-Reynolds-number turbulence model as two separate issues. The strongest argument in favor of this approach is simply that all spectral effects are lost in the time-averaging process used by turbulence models. Tollmien-Schlichting waves, for example, cannot be distinguished by a turbulence model. Since a given boundary layer is unstable to perturbations that fall in a specific range of frequencies, conventional turbulence models, which distinguish only magnitude and an average frequency, can never be certain if a given perturbation will actually cause transition. However, if we implement two separate models, one for the transition region and another for the developing turbulent region, achieving a smooth joining of the two models' predictions presents an additional complication. This complication can be avoided if we view both issues as low-Reynolds-number phenomena that can be addressed in the context of a single model. The strongest argument for this approach is that we can use the same model to describe a smooth transition from laminar to fully turbulent flow, including the transitional region. This approach is plausible provided we restrict our applications to broadband transition-triggering disturbances.

Nevertheless, there should be no pretense that this approach has sufficient physical foundation to describe the onset of transition. The conceptual reason for this reservation is as follows. Using the single length scale implied by a typical two-equation turbulence model is much less satisfactory for transitional flows than for turbulent flows. That is, production and dissipation processes come from different parts of the turbulence spectrum. Large eddies are primarily responsible for production, whereas the smallest eddies dissipate turbulence energy into internal energy. In a turbulent flow, the largest eddies also control the rate of dissipation by way of the cascading of energy down the spectrum to the smallest eddies. That is, there is a degree of universality to the turbulence spectrum for turbulent flows, provided the Reynolds number is large enough to permit a distinct inertial subrange. By contrast, it is very unlikely that such a universal spectrum exists in a transitional flow, and certainly not in the earliest stages of transition.

These considerations needn't deter us from attempting to use turbulence models to predict transitional flows since, for most applications, even cruder correlation methods are often used. Two-equation turbulence models appear to give useful results for a much wider range of turbulent flows than we have any right to expect. But how much more surprising is this than the great success enjoyed by the classical Smith-Van Ingen[1] e^n method whose physical foundation is nonexistent? In other words, clever engineering approximations often exceed our expectations.

Our best hope of success is in describing the nonlinear growth of disturbances once transition has begun. Using linear stability theory to compute the closure coefficients in a two-equation turbulence model for a transitional boundary layer, Wilcox[2] has shown that spectral effects are unimportant after the initial disturbance has been amplified by a factor of only e^4. The research of Wilcox et al.[3–7] provides a great deal of support for the turbulence-model approach. Using a k-ω^2 turbulence model and transition-specific, low-Reynolds-number modifications, Wilcox simulated boundary-layer transition for a wide range of Mach numbers including pressure gradient, surface roughness, surface heating and cooling, and surface mass transfer. The purpose of this paper is to build on the aforementioned work, taking advantage of recent direct numerical simulation (DNS) results in developing appropriate viscous modifications for the Wilcox[8] k-ω model.

In contrast to the earlier research, however, no attempt is made in this paper to develop a general procedure for predicting the onset of transition. Rather, the emphasis is on predicting flow in the transition region. This is an easier problem and one that is more amenable to solution with a turbulence model. In this spirit, Sec. V presents a new method for triggering transition at a specified location.

For general compressible flows, the complete set of equations that constitute the low-Reynolds-number k-ω two-equation model developed and tested in this paper are as follows.

$$\frac{\partial \rho}{\partial t} + \frac{\partial}{\partial x_i}(\rho u_i) = 0 \tag{1}$$

$$\frac{\partial}{\partial t}(\rho u_i) + \frac{\partial}{\partial x_j}(\rho u_j u_i) = \frac{\partial}{\partial x_j}(-p\delta_{ji} + \hat{\tau}_{ji}) \tag{2}$$

Received Oct. 16, 1992; revision received July 20, 1993; accepted for publication Aug. 16, 1993.

*President, 5354 Palm Drive. Associate Fellow AIAA.

$$\frac{\partial}{\partial t}(\rho k) + \frac{\partial}{\partial x_j}(\rho u_j k) = \tau_{ij}\frac{\partial u_i}{\partial x_j} - \beta^*\rho\omega k + \frac{\partial}{\partial x_j}\left[(\mu + \sigma^*\mu_T)\frac{\partial k}{\partial x_j}\right] \tag{3}$$

$$\frac{\partial}{\partial t}(\rho\omega) + \frac{\partial}{\partial x_j}(\rho u_j \omega) = \alpha\frac{\omega}{k}\tau_{ij}\frac{\partial u_i}{\partial x_j} - \beta\rho\omega^2 + \frac{\partial}{\partial x_j}\left[(\mu + \sigma\mu_T)\frac{\partial \omega}{\partial x_j}\right] \tag{4}$$

$$\hat{\tau}_{ij} = 2\mu\left(S_{ij} - \frac{1}{3}\frac{\partial u_k}{\partial x_k}\delta_{ij}\right) + \tau_{ij} \tag{5}$$

$$\tau_{ij} = 2\mu_T\left(S_{ij} - \frac{1}{3}\frac{\partial u_k}{\partial x_k}\delta_{ij}\right) + -\frac{2}{3}\rho k\delta_{ij} \tag{6}$$

$$\mu_T = \alpha^*\rho k/\omega \tag{7}$$

$$S_{ij} = \frac{1}{2}\left(\frac{\partial u_i}{\partial x_j} + \frac{\partial u_j}{\partial x_i}\right) \tag{8}$$

In Eqs. (1–8), t is time, x_i is position vector, u_i is velocity, ρ is density, p is pressure, μ is molecular viscosity, and $\hat{\tau}_{ij}$ is the sum of molecular and Reynolds stress tensors. Also, δ_{ij} is the Kronecker delta, k is the turbulence kinetic energy, ω is specific dissipation rate, τ_{ij} is Reynolds stress tensor, and μ_T is eddy viscosity. The six parameters α^*, α, β^*, β, σ^*, and σ are closure coefficients whose values are given next:

$$\alpha^* = \frac{\alpha_o^* + Re_T/R_k}{1 + Re_T/R_k} \tag{9}$$

$$\alpha = \frac{5}{9}\cdot\frac{\alpha_o + Re_T/R_\omega}{1 + Re_T/R_\omega}\cdot(\alpha^*)^{-1} \tag{10}$$

$$\beta^* = \frac{9}{100}\cdot\frac{5/18 + (Re_T/R_\beta)^4}{1 + (Re_T/R_\beta)^4} \tag{11}$$

$$\beta = 3/40, \qquad \sigma^* = \sigma = 1/2 \tag{12}$$

$$\alpha_o^* = \beta/3, \qquad \alpha_o = 1/10 \tag{13}$$

$$R_\beta = 8, \qquad R_k = 6, \qquad R_\omega = 2.7 \tag{14}$$

where Re_T is the turbulence Reynolds number defined by

$$Re_T = \frac{\rho k}{\omega\mu} \tag{15}$$

Section II explains in detail how the turbulence model simulates transition, and justifies the form of the viscous modifications. Section III demonstrates how well the model performs for low-Reynolds-number channel flow and for pipe flow. Section IV includes transition predictions for an incompressible flat-plate boundary layer. Section V discusses a new method for triggering transition and includes additional transition applications. Section VI presents a summary of and conclusions drawn from the study.

II. Simulating Transition with the k-ω Model

Turbulence model equations can be used to predict transition from laminar to turbulent flow, although most models predict transition to turbulence at Reynolds numbers that are at least an order of magnitude too low. To understand why and how the k-ω model predicts transition, consider the flat-plate boundary layer. For an incompressible, two-dimensional boundary layer, the equations for k and ω are as follows:

$$u\frac{\partial u}{\partial x} + v\frac{\partial u}{\partial y} = \frac{\partial}{\partial y}\left[(\nu + \nu_T)\frac{\partial u}{\partial y}\right] \tag{16}$$

$$u\frac{\partial k}{\partial x} + v\frac{\partial k}{\partial y} = \nu_T\left(\frac{\partial u}{\partial y}\right)^2 - \beta^*\omega k + \frac{\partial}{\partial y}\left[(\nu + \sigma^*\nu_T)\frac{\partial k}{\partial y}\right] \tag{17}$$

$$u\frac{\partial \omega}{\partial x} + v\frac{\partial \omega}{\partial y} = \alpha\frac{\omega}{k}\nu_T\left(\frac{\partial u}{\partial y}\right)^2 - \beta\omega^2 + \frac{\partial}{\partial y}\left[(\nu + \sigma\nu_T)\frac{\partial \omega}{\partial y}\right] \tag{18}$$

$$\nu_T = \alpha^* k/\omega \tag{19}$$

where u and v are velocity components in the streamwise x and normal y directions, respectively, ν is kinematic molecular viscosity, and ν_T is kinematic eddy viscosity. We can most clearly illustrate how the model equations predict transition by rearranging terms in Eqs. (17) and (18) as follows:

$$u\frac{\partial k}{\partial x} + v\frac{\partial k}{\partial y} = P_k\beta^*\omega k + \frac{\partial}{\partial y}\left[(\nu + \sigma^*\nu_T)\frac{\partial k}{\partial y}\right] \tag{20}$$

$$u\frac{\partial \omega}{\partial x} + v\frac{\partial \omega}{\partial y} = P_\omega\beta\omega^2 + \frac{\partial}{\partial y}\left[(\nu + \sigma\nu_T)\frac{\partial \omega}{\partial y}\right] \tag{21}$$

The net production per unit dissipation for the two equations, P_k and P_ω, are defined by

$$P_k = \frac{\alpha^*}{\beta^*}\left(\frac{\partial u/\partial y}{\omega}\right)^2 - 1 \tag{22}$$

$$P_\omega = \frac{\alpha\alpha^*}{\beta}\left(\frac{\partial u/\partial y}{\omega}\right)^2 - 1 \tag{23}$$

There are two important observations worthy of mention at this point. First, if the turbulence energy is zero, Eq. (21) has a well-behaved solution. That is, when $k = 0$, the eddy viscosity vanishes and the ω equation uncouples from the k equation. Consequently, the k-ω model has a nontrivial laminar-flow solution for ω. Second, the signs of P_k and P_ω determine whether k and ω are amplified or reduced in magnitude. However, it is not obvious by inspection of Eqs. (22) and (23) how the signs of these terms vary with Reynolds number as we move from the plate leading edge to points downstream. We can make the variation obvious by rewriting Eqs. (22) and (23) in terms of the Blasius transformation.

Before we introduce the Blasius transformation, we must determine the appropriate scaling for ω. To do this, we note that, close to the surface of a perfectly smooth flat plate, the specific dissipation rate behaves according to[8] (see Wilcox[9] for a complete discussion of how this behavior can be accommodated numerically)

$$\omega \to \frac{6\nu}{\beta y^2} \quad \text{as} \quad y \to 0 \tag{24}$$

In terms of the Blasius similarity variable η, defined by

$$\eta = y\sqrt{\frac{U_\infty}{\nu x}} \tag{25}$$

where U_∞ is freestream velocity, the asymptotic behavior of ω approaching the surface is

$$\eta \to \frac{6}{\beta}\frac{U_\infty}{x}\frac{1}{\eta^2} \quad \text{as} \quad \eta \to 0 \tag{26}$$

Consequently, we conclude that the appropriate scaling for ω in the Blasius boundary layer is given by

$$\omega = \frac{U_\infty}{x} W(\eta) \tag{27}$$

where $W(\eta)$ is a dimensionless function to be determined as part of the solution. Hence, if we write the velocity in terms of dimensionless velocity, $\mathcal{U}(\eta)$, i.e.,

$$u = U_\infty \mathcal{U}(\eta) \tag{28}$$

the net production per unit dissipation terms become

$$P_k = \frac{\alpha^*}{\beta^*} Re_x \left(\frac{\partial \mathcal{U}/\partial \eta}{W} \right)^2 - 1 \tag{29}$$

$$P_\omega = \frac{\alpha\alpha^*}{\beta} Re_x \left(\frac{\partial \mathcal{U}/\partial \eta}{W} \right)^2 - 1 \tag{30}$$

Thus, both P_k and P_ω increase linearly with Reynolds number, Re_x. From the exact laminar solution for $\mathcal{U}(\eta)$ and $W(\eta)$, the maximum value of the ratio of $\partial \mathcal{U}/\partial \eta$ to W is given by

$$\left(\frac{\partial \mathcal{U}/\partial \eta}{W} \right)_{\max} \approx \frac{1}{300} \tag{31}$$

The precise value of this ratio is actually a weak function of the freestream value of ω, ranging between 0.0025 and 0.0040. The maximum occurs about midway through the boundary layer ($y/\delta = 0.56$), a point above which the exact near-wall behavior of ω [Eq. (24)] does not hold. Hence, a complete boundary-layer solution has been used to determine the maximum ratio of $\partial \mathcal{U}/\partial \eta$ to W.

Hence, as long as the eddy viscosity remains small compared with the molecular viscosity, we can specify the precise points where P_k and P_ω change sign. In general, using Eq. (31), we conclude that the sign changes occur at the following Reynolds numbers:

$$(Re_x)_k = 9 \cdot 10^4 \frac{\beta^*}{\alpha^*} \tag{32}$$

$$(Re_x)_w = 9 \cdot 10^4 \frac{\beta}{\alpha\alpha^*} \tag{33}$$

With no viscous modifications, the closure coefficients α^*, α, β^*, and β are 1, 5/9, 9/100, and 3/40, respectively. These values correspond to the limiting form of Eqs. (9–14) as $Re_T \to \infty$. Using these fully turbulent values, we find $(Re_x)_k = 8.1 \times 10^3$ and $(Re_x)_\omega = 1.215 \times 10^4$. Thus, starting from laminar flow at the leading edge of a flat plate (see Fig. 1), the following sequence of events occurs.

1) The computation starts in a laminar region with $k = 0$ in the boundary layer and a small freestream value of k.

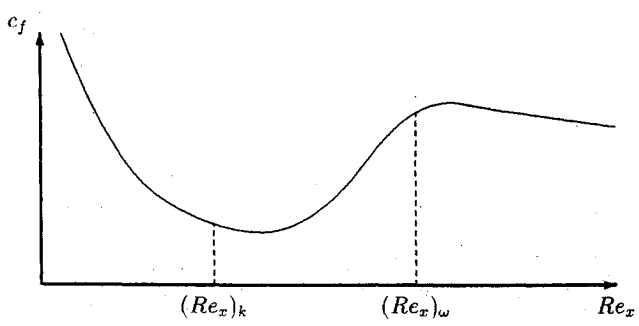

Fig. 1 Skin friction variation for a boundary layer undergoing transition from laminar to turbulent flow.

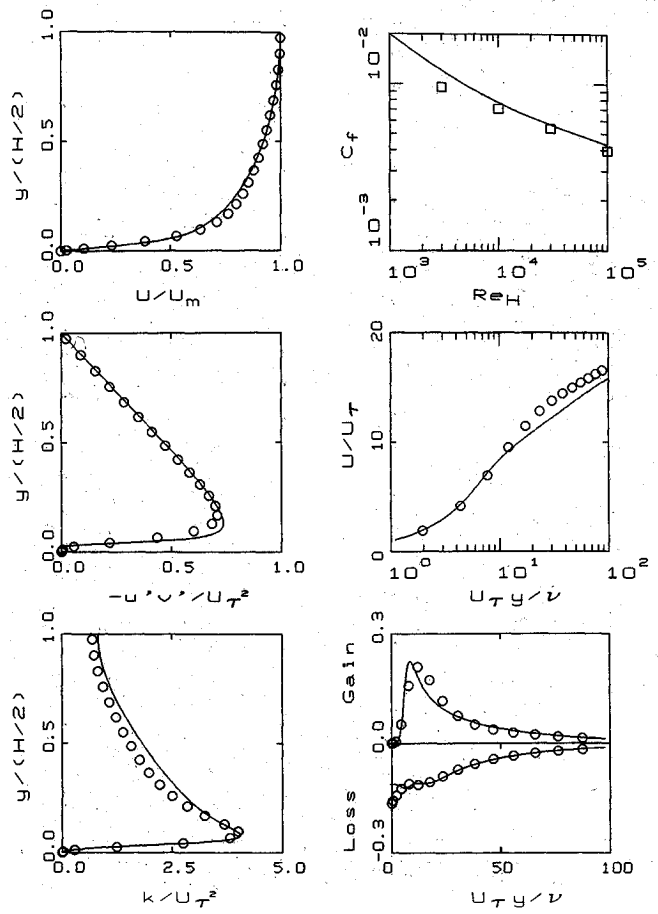

Fig. 2 Incompressible channel flow with $Re_\tau = 1.8 \times 10^2$, $Re_H = 5.59 \times 10^3$; ○, Mansour et al.; □, Halleen-Johnston formula; ——, computed.

2) Initially, because $P_k < 0$ and $P_\omega < 0$, dissipation of both k and ω exceeds production. Turbulence energy is entrained from the freestream and spreads through the boundary layer by molecular diffusion. Neither k nor ω is amplified and the boundary layer remains laminar.

3) At the critical Reynolds number, $Re_{x_c} = 8.1 \times 10^3$, production overtakes dissipation in the k equation. Downstream of x_c, production exceeds dissipation in the k equation, and turbulence energy is amplified. At some point in this process, the eddy viscosity grows rapidly, and this corresponds to the transition point.

4) The k continues to be amplified, and beyond $Re_x = 1.215 \times 10^4$, production catches dissipation in the ω equation. Now ω is amplified and continues growing until a balance between production and dissipation is achieved in the k equation. When this balance is achieved, transition from laminar to turbulent flow is complete.

Consistent with experimental measurements, the entire process is very sensitive to the freestream value of k. There is also a sensitivity to the freestream value of ω, although the sensitivity is more difficult to quantify.

Three key points are immediately obvious. First, k begins growing at a Reynolds number of 8.1×10^3. By contrast, linear-stability theory tells us that Tollmien-Schlichting waves begin forming in the Blasius boundary layer at a Reynolds number of 9×10^4. This is known as the minimum critical Reynolds number. Correspondingly, we find that the model predicts transition at much too low a Reynolds number. Second, inspection of Eqs. (32) and (33) shows that the width of the transition region is controlled by the ratio of β to $\alpha\alpha^*$. Third, transition will never occur if P_ω reaches zero earlier than P_k. Thus, occurrence of transition requires

$$\alpha\alpha^* < \alpha^*\beta/\beta^* \quad \text{as} \quad Re_T \to 0 \tag{34}$$

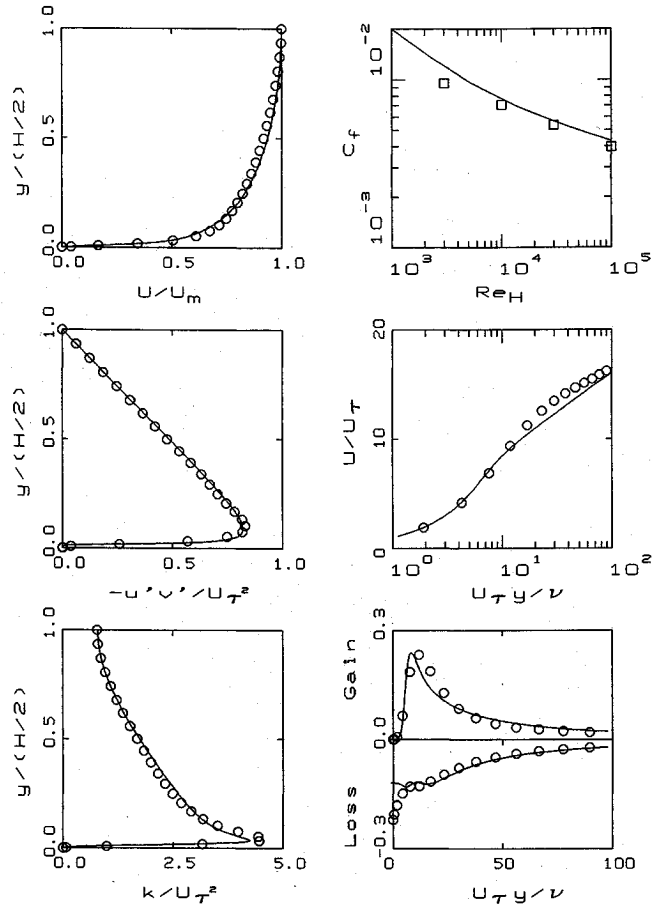

Fig. 3 Incompressible channel flow with $Re_\tau = 3.95 \times 10^2$, $Re_H = 1.375 \times 10^4$; o, Mansour et al.; □, Halleen-Johnston formula; ——, computed.

This fact must be preserved in any viscous modification to the model. The viscous modifications in Eqs. (9–14), i.e., the dependence of α, α^*, and β^* on Re_T, are designed to accomplish two objectives. The most important objective is to match the minimum critical Reynolds number. Reference to Eq. (32) shows that we must require

$$\beta^*/\alpha^* \to 1 \qquad \text{as} \qquad Re_T \to 0 \tag{35}$$

A secondary objective is to achieve asymptotic consistency with the exact behavior of k and dissipation, $\epsilon = \beta^* k\omega$, approaching a solid boundary. That is, we would like to have

$$k/y^2 \to \text{const}, \qquad \epsilon/k \to 2\nu/y^2 \qquad \text{as} \qquad y \to 0 \tag{36}$$

Close to a solid boundary, Wilcox[8] shows that the dissipation and molecular diffusion terms balance in both the k and ω equations. The very-near-wall solution for ω is given by Eq. (24). The solution for k is of the form

$$k/y^n \to \text{const} \qquad \text{as} \qquad y \to 0 \tag{37}$$

where n is given by

$$n = \tfrac{1}{2}\left[1 + \sqrt{1 + 24\beta^*/\beta}\right] \tag{38}$$

Noting that dissipation is related to k and ω by

$$\epsilon = \beta^* k\omega \tag{39}$$

we can achieve the desired asymptotic behavior of Eq. (36) by requiring

$$\beta^*/\beta \to 1/3 \qquad \text{as} \qquad Re_T \to 0 \tag{40}$$

Requiring this limiting behavior as $Re_T \to 0$ is sufficient to achieve the desired asymptotic behavior as $y \to 0$ since the eddy viscosity, and hence, Re_T vanish at a solid boundary.

If we choose to have β constant for all values of Re_T, Eqs. (34), (35), and (40) are sufficient to determine the limiting values of α^* and β^* and an upper bound for $\alpha\alpha^*$ as turbulence Reynolds number becomes vanishingly small. Specifically, we find

$$\left.\begin{aligned} &\alpha\alpha^* < \beta \\ &\alpha^* \to \beta/3 \\ &\beta^* \to \beta/3 \end{aligned}\right\} \qquad \text{as} \qquad Re_T \to 0 \tag{41}$$

Wilcox[3–5] and Chambers and Wilcox[6] make the equivalent of $\alpha\alpha^*$ and α^* in their k-ω^2 models approach the same limiting value and obtain excellent agreement with measured transition width for incompressible boundary layers. Numerical experimentation with the k-ω model indicates the optimum choice for incompressible boundary layers is $\alpha\alpha^* \to 0.74\beta$, or

$$\alpha\alpha^* \to 1/18 \qquad \text{as} \qquad Re_T \to 0 \tag{42}$$

Equations (9–14) postulate functional dependencies on Re_T that guarantee the limiting values in Eqs. (41) and (42), as well as the original fully turbulent values for $Re_T \to \infty$.

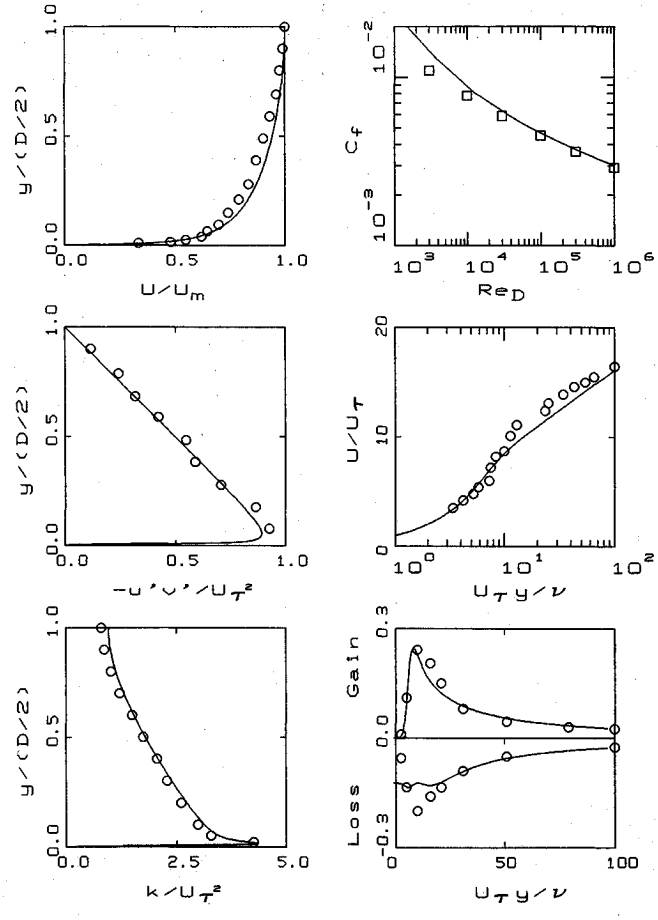

Fig. 4 Incompressible pipe flow with $Re_\tau = 1.058 \times 10^3$, $Re_R = 4.0 \times 10^4$; o, Laufer; □, Prandtl formula; ——, computed.

The three coefficients R_β, R_k, and R_ω control the rate at which the closure coefficients approach their fully turbulent values. As in previous analyses based on the k-ω model,[8-11] we can determine their values by using perturbation methods to analyze the viscous sublayer. Using the well-established procedure, we can solve for the constant in the law of the wall B by solving the sublayer equations and evaluating the following limit:

$$B = \lim_{y \to \infty} \left(u^+ - \frac{1}{\kappa} \ell n\, y^+ \right) \tag{43}$$

where $u^+ = u/u_\tau$ and $y^+ = u_\tau y/\nu$ are standard sublayer scaled coordinates. Also, $\kappa = 0.41$ is von Kármán's constant. For a given value of R_β and R_k, there is a unique value of R_ω that yields a constant in the law of the wall of 5.0. For small values of R_β the peak value of k near the surface is close to the value achieved without viscous corrections, viz., $u_\tau^2/\sqrt{\beta^*}$. As R_β increases, the maximum value of k near the surface increases. Comparison of computed sublayer structure with direct numerical simulation (DNS) results of Mansour et al.[12] indicates the optimum choice for these three coefficients is as indicated in Eq. (14). Section III presents a complete comparison of computed channel flow properties with the DNS results of Mansour et al.[12]

The only flaw in the model's near-wall asymptotic consistency occurs in the Reynolds shear stress τ_{xy}. Although the exact asymptotic behavior is $\tau_{xy} \sim y^3$, the model as formulated predicts $\tau_{xy} \sim y^4$.

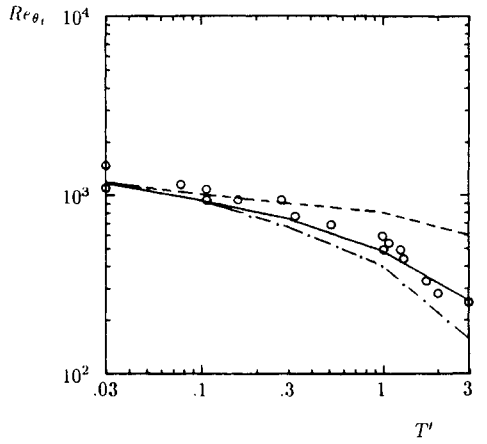

Fig. 5 Transition location for an incompressible flat-plate boundary layer; - - -, $\ell/\delta = 0.001$; ——, $\ell/\delta = 0.010$; – · –, $\ell/\delta = 0.100$; o, Dryden.

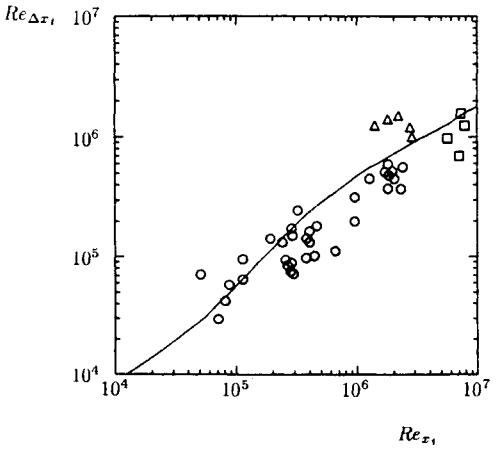

Fig. 6 Transition width for an incompressible flat-plate boundary layer; o, Dhawan-Narasimha; Δ, Schubauer-Skramstad; □, Fisher-Dougherty; ——, computed.

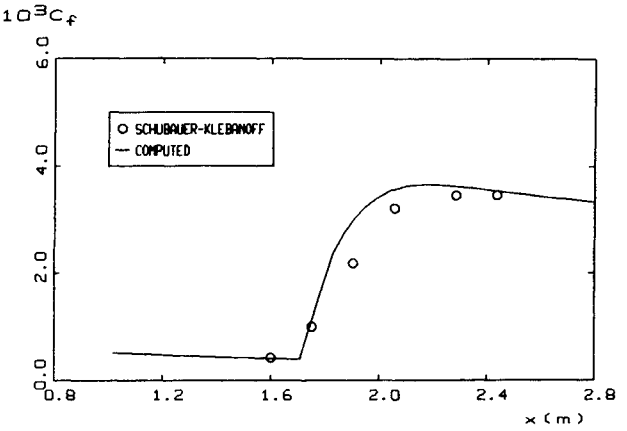

Fig. 7 Transitional incompressible flat-plate boundary layer.

This discrepancy could easily be removed with another viscous modification. However, results obtained to date indicate this is of no significant consequence. It has no obvious bearing on either the model's ability to predict transition or properties of interest in turbulent boundary layers. The additional complexity and uncertainty involved in achieving this subtle feature of the very near wall behavior of τ_{xy} does not appear to be justified.

III. Channel and Pipe Flow

To achieve a complete description of the transition from laminar to turbulent flow, we must be able to accurately describe the flow in the turbulent regime. This is, after all, the primary advantage of using turbulence model equations to describe transition. In this section, we examine channel and pipe flow to demonstrate how well the low-Reynolds-number form of the k-ω model predicts properties of turbulent flows. All computations in this section have been done using a highly accurate one-dimensional time-marching program (PIPE) documented by Wilcox.[9]

Figures 2 and 3 compare computed channel-flow skin friction c_f with the Halleen and Johnston[13] correlation for Reynolds number based on channel height H and average velocity ranging from 10^3 to 10^5. The correlation is

$$c_f = 0.0706\, Re_H^{-1/4} \tag{44}$$

As shown, computed c_f differs from the correlation by less than 3% except at the lowest Reynolds number shown where the correlation probably is inaccurate. Figure 4 compares computed pipe flow c_f with Prandtl's universal law of friction, viz.,

$$\frac{1}{\sqrt{c_f}} = 4 \log_{10}(2Re_D\sqrt{c_f}) - 1.6 \tag{45}$$

Reynolds number based on pipe diameter D and average velocity varies from 10^3 to 10^6. As with channel flow, computed c_f falls within 5% of the correlation except at the lowest Reynolds number indicated where the correlation is likely to be in error.

For more detailed comparisons, we consider two low-Reynolds-number channel-flow cases corresponding to the DNS results of Mansour et al.[12] and one high-Reynolds-number pipe flow case corresponding to measurements of Laufer.[14]

For purposes of identification, the three cases are referred to in terms of the parameter

$$Re_\tau = u_\tau R/\nu \tag{46}$$

where u_τ is friction velocity and R is either channel half-height or pipe radius. Figures 2 and 3 compare various computed profiles with the DNS results of Mansour et al.[12] for $Re_\tau = 1.8 \times 10^2$ and 3.95×10^2, respectively.

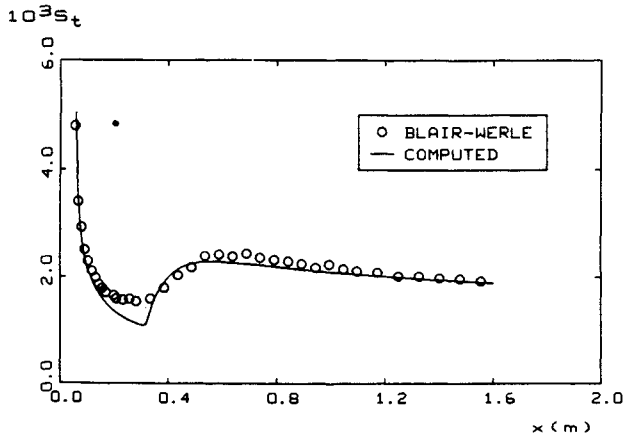

Case 1: Mildly favorable pressure gradient

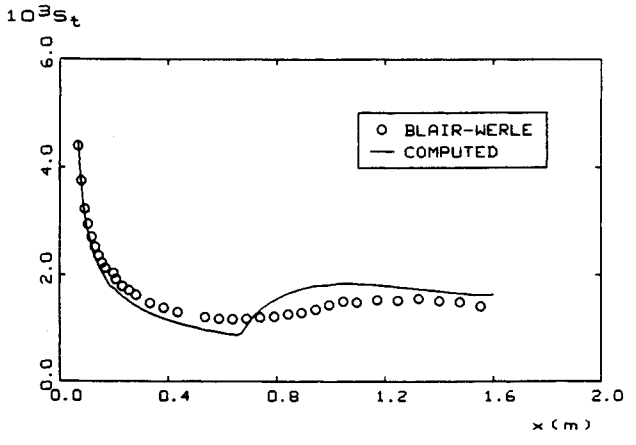

Case 2: Strongly favorable pressure gradient

Fig. 8 Transitional incompressible boundary-layer flow with favorable pressure gradient and surface cooling.

Six different comparisons are shown in each figure, including mean velocity, skin friction, Reynolds shear stress, turbulence kinetic energy, turbulence energy production, and dissipation rate. For both cases, velocity, Reynolds shear stress, and turbulence kinetic energy profiles differ by less than 7%. Most notably, for both Reynolds numbers, the model predicts the peak value of k near the channel wall to within 4% of the DNS value. Additionally, approaching the surface, the turbulence-energy production $\tau_{xy}\partial U/\partial y$ and dissipation ϵ are within 10% of the DNS results except very close to the surface.

Figure 4 compares k-ω model pipe flow results with Laufer's[14] measurements at a Reynolds number based on pipe diameter and average velocity of 4×10^4. As shown, computed and measured velocity and Reynolds shear stress profiles differ by less than 8%. As with channel flow, computed and measured turbulence kinetic energy differ by about 5%, including close to the surface where the sharp peak occurs. Note that, at this high a Reynolds number, the k profile has a sharp spike near $y = 0$ and this feature is captured in the computations. Except very close to the surface, computed turbulence energy production and dissipation differ from measured values by less than 10%. This may actually be a desirable result. That is, some controversy exists about the accuracy of Laufer's dissipation measurements close to the surface.

IV. Transitional Flat-Plate Boundary Layer

Figure 5 compares computed and measured transition Reynolds number, $Re_{\theta t}$, for an incompressible flat-plate boundary layer. Computations have been performed using program EDDYBL, the two-dimensional compressible boundary-layer program documented by Wilcox.[9] We define the transition Reynolds number as the point where the skin friction achieves its minimum value. Results are displayed as a function of freestream turbulence intensity T' defined by

$$T' = 100\sqrt{\frac{2}{3}\frac{k_e}{U_e^2}} \tag{47}$$

where subscript e denotes the value at the boundary-layer edge. As shown, consistent with the data compiled by Dryden,[15] $Re_{\theta t}$ increases as the freestream intensity decreases. Because ω can be thought of as an averaged frequency of the freestream turbulence, it is reasonable to expect the predictions to be sensitive to the freestream value of ω. To assess the effect, the freestream value of the turbulence length scale defined by $\ell = k^{1/2}/\omega$ has been varied from 0.001δ to 0.100δ where δ is boundary layer thickness. As shown, computed $Re_{\theta t}$ values bracket virtually all of the data. Note that the k-ω model's sensitivity to the freestream value of ω is a desirable feature for transition applications. Physical transition location is not simply a function of T' but rather is frequency dependent. Although it is unclear how the freestream value of ω should be specified, consistent with measurements, the model is not confined to a single transition location for a given T' regardless of the frequency of the disturbance.

Figure 6 compares computed transition width with measurements.[16-18] We define transition width Δx_t as the distance between minimum and maximum skin-friction points. The computed width falls within experimental data scatter for $Re_{x_t} < 10^6$ and lies a bit below the data for larger values. The Δx_t is unaffected by the freestream value of ω.

V. Numerical Roughness Strip

In formulating the low-Reynolds-number k-ω model, we have only guaranteed that the point where k is first amplified matches the minimum critical Reynolds number for the incompressible, flat-plate boundary layer. To simulate transition with complicating effects such as pressure gradient, surface heat transfer, surface roughness, compressibility, etc., the values of α_o^* and α_o must change.[6] Their values can be deduced from linear-stability theory results or perhaps from a correlation based on stability theory. Nevertheless, some information must be provided about the minimum critical Reynolds number for each new application. As noted in the Introduction, Wilcox[2] has shown that, after a disturbance has grown to a factor of e^4 times its initial value, the turbulence model closure coefficients lose all memory of spectral effects. Thus, we can conclude that, not far downstream of the minimum critical Reynolds number, Reynolds averaging is sensible. Consequently, the most practical way to use the model for transitional flows is in describing the transitional region.

For any flow, we can always match the measured transition point by adjusting the freestream value of k. This is satisfactory when the transition point occurs at a large Reynolds number, which requires k_∞ to be small relative to U_∞^2. However, for high-speed flows in which transition often occurs at a relatively small Reynolds number, we have found that unreasonably large values of k_∞ are needed to trigger transition, so large as to affect the total energy in the freestream in a physically unrealistic manner. Thus, a new method for triggering transition is needed.

To devise an alternative method, we can take advantage of a unique feature of the k-ω model. Specifically, by using a finite value for ω at the surface, we can simulate surface roughness with the model. For fully turbulent boundary layers, Wilcox[8] shows that

Table 1 Results for Schubauer-Skramstad test cases

Case	Re_{x_t}	$(Re_{\Delta x_t})_{\text{computed}}$	$(Re_{\Delta x_t})_{\text{computed}}$
1	2.85×10^6	0.88×10^6	1.00×10^6
2	2.75×10^6	0.86×10^6	1.20×10^6
3	2.20×10^6	0.78×10^6	1.50×10^6
4	1.80×10^6	0.69×10^6	1.40×10^6
5	1.40×10^6	0.58×10^6	1.25×10^6

$$\omega = \frac{u_\tau^2}{\nu} S_R \qquad \text{at} \qquad y = 0 \tag{48}$$

where S_R is a dimensionless function of the surface roughness height k_R, defined by (with $k_R^+ = u_\tau k_R/\nu$)

$$S_R = \begin{cases} (50/k_R^+)^2 & k_R^+ < 25 \\ 100/k_R^+ & k_R^+ \geq 25 \end{cases} \tag{49}$$

If a smooth surface is desired, the value of k_R is selected to insure that $k_R^+ < 5$, which corresponds to a so-called "hydraulically smooth" surface.

Since increasing the surface roughness height corresponds to decreasing the surface value of ω (and thus the dissipation in the k equation), the model predicts that roughness will have a destabilizing effect. This is consistent with measurements, and patches of surface roughness are often used to trigger transition in experiments. Thus, a possible way to trigger transition with the model

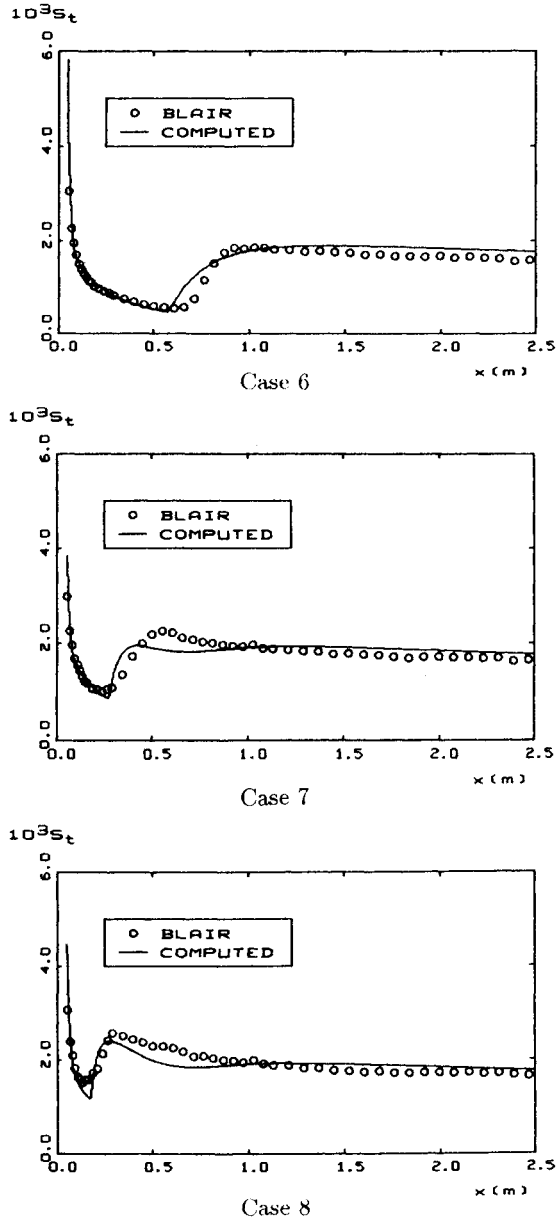

Fig. 9 Transition width for flat-plate boundary layers with surface heat transfer.

Table 2 Results for Fisher-Dougherty test cases

Case	Mach no.	Re_{x_t}	$Re_{\Delta x_t}$	$(Re_{\Delta x_t})_{\text{exp}}$
1	1.16	7.02×10^6	0.89×10^6	0.69×10^6
2	1.30	5.61×10^6	0.84×10^6	0.97×10^6
3	1.55	7.89×10^6	1.08×10^6	1.24×10^6
4	1.86	7.29×10^6	1.07×10^6	1.56×10^6

equations is to numerically simulate a roughness strip via Eqs. (48) and (49).

We have run 18 two-dimensional and axisymmetric transitional boundary-layer cases to test this idea. We have been able to trigger transition at the desired location for all of the cases considered using a roughness strip with k_R and the streamwise extent of the strip Δs given by the following correlations:

$$\frac{k_R}{\delta_t} = \max\left\{\frac{5000}{\sqrt{Re_{s_t}}}, 3\right\} \tag{50}$$

$$\frac{\Delta s}{\delta_t} = 0.015\sqrt{Re_{s_t}} \tag{51}$$

The quantities δ_t and Re_{s_t} are the boundary-layer thickness and transition Reynolds number based on arc length.

In all cases, again using program EDDYBL, computation begins at the plate leading edge, and the turbulence kinetic energy is initially set to an extremely small value, viz., $10^{-15} U_\infty^2$, throughout the boundary layer. This value is too small to trigger transition naturally. The initial ω profile is given by the exact laminar-flow solution to the model equations. The surface is assumed to be perfectly smooth ($k_R^+ \ll 1$) everywhere outside of the numerical roughness strip.

Incompressible Flat Plate

The first case is flow 1 from Singer et al.[19] This is an incompressible flat-plate boundary layer that undergoes transition at a plate length between 1.6 and 1.8 m. According to Eqs. (50) and (51), this flow requires a roughness strip with $k_R/\delta_t = 3.0$ and $\Delta s/\delta_t = 25$. Numerical experimentation shows that a shorter transition strip, i.e., $\Delta s/\delta_t = 7$, is sufficient to trigger transition at the desired location for this case. Figure 7 compares computed and measured[20] skin friction throughout the transition region. Computed and measured c_f differ by less than 16% of the peak skin friction.

Favorable Pressure Gradient Boundary Layers

The next applications are for incompressible boundary layers in a favorable pressure gradient. The boundary layers considered correspond to flow 2/cases 1 and 2 of Singer et al. In addition to having adverse pressure gradient, the surface is cooled. Figure 8 compares computed and measured[21] Stanton numbers for the two cases. Case 2 has a stronger favorable pressure gradient than case 1. The dimensions of the roughness strip required to match the measured transition point are $(k_R/\delta_t, \Delta s/\delta_t) = (10, 10)$ and $(4, 9)$, respectively, for cases 1 and 2. Equations (50) and (51) indicate $(k_R/\delta_t, \Delta s/\delta_t) = (8.5, 8.7)$ and $(6.0, 12.5)$, respectively.

Freestream Turbulence Effects

We turn now to effects of freestream turbulence, i.e., flow 4 of the study by Singer et al. All of the cases considered are for incompressible boundary layers; three cases include surface heat transfer. Table 1 shows that the computed transition width for cases 1–5 is consistently smaller than measured[17]; the data are included in Fig. 6. For cases 6–8, Fig. 9 shows that the predicted peak Stanton number is about 10–15% lower than measured.[22]

Supersonic Cone Flow

For this application we consider flow 3 of the study by Singer et al. Cases 1–4 focus on flow past a 5-deg half-angle cone with

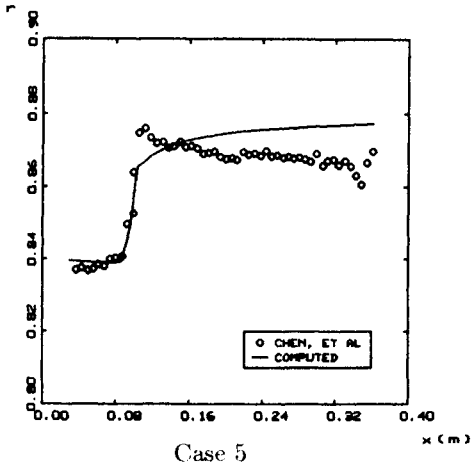

Case 5

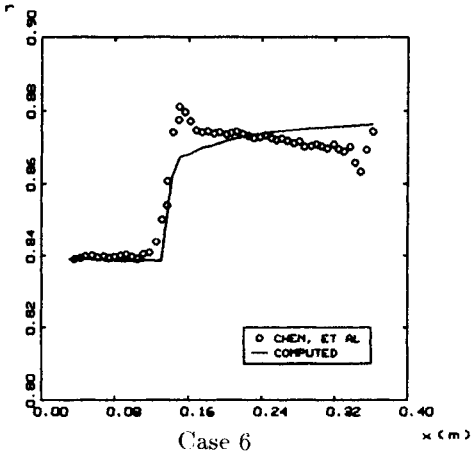

Case 6

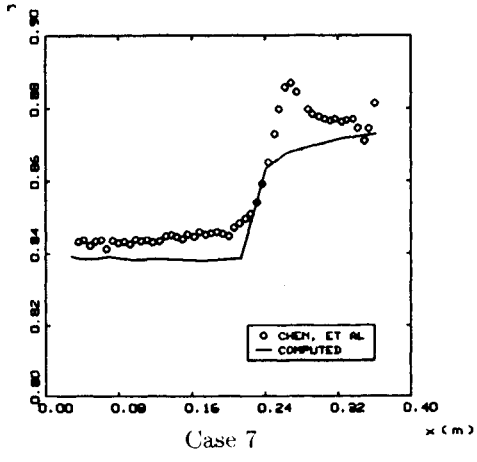

Case 7

Fig. 10 Transitional flow on a 5-deg half-angle, adiabatic cone at Mach 3.36.

Mach numbers ranging from 1.16 to 1.86, corresponding to measurements of Fisher and Dougherty.[18] Measurements are available only for the beginning and end of transition. Table 2 summarizes the transition Reynolds number Re_{x_t} and the Reynolds number based on transition width $Re_{\Delta x_t}$; the data are included in Fig. 6.

Cases 5–7 are for Mach 3.36 flow past a 5 deg half-angle cone, with an adiabatic surface. The three cases considered have different unit Reynolds numbers. Figure 10 compares computed and measured[23] recovery factor r for the three cases. Note that unit Reynolds number is smallest for case 5 and largest for case 7. Interestingly, consistent with measurements, the asymptotic value of the recovery factor is about 0.875 for all three cases compared with the generally accepted value of 0.89. As a simple numerical experiment, we have run these computations without transverse curvature, i.e., as two-dimensional flows. The predicted asymptotic value of the recovery factor is 0.89.

VI. Summary and Conclusions

We have made important progress in developing a transition model. Sections III–V show that the low-Reynolds-number k-ω model provides a reasonably accurate description for fully developed turbulent channel and pipe flow and for several transitional boundary layers.

In the context of turbulent boundary layers, Sec. III shows that the low-Reynolds-number version of the model retains all of the best features of the baseline, high-Reynolds-number version of the model. Most notably, the model is just as accurate as the baseline model for channel and pipe flow and even describes subtle near-wall features. This guarantees that the model approaches the correct post-transition, asymptotic state.

In the context of transitional boundary layers, Sec. IV shows that, although the low-Reynolds number k-ω model offers realistic predictions, more development is needed to achieve close quantitative agreement with measurements. Most importantly, transition width is close to measured width for low transition Reynolds numbers. At higher transition Reynolds numbers, model-predicted transition is more abrupt than measured.

Results of Sec. V show that the new transition-triggering method is very effective. Equation (50) is an upper bound for the roughness height required to trigger transition for all of the cases considered. In many cases, a smaller roughness height is sufficient, and the user should try different roughness heights, if possible, to determine the optimum height for a given application. Equation (51) is less certain. The formula also expresses an upper bound that covers all of the cases considered. The actual values used permit the roughness strip to persist for at least three streamwise finite difference cells.

On balance, although there is room for improvement, the applications presented in Secs. III–V indicate we have formed a solid foundation for future low-Reynolds-number and transition research.

Acknowledgments

This research was supported by the U.S. Army Research Office and the NASA Langley Research Center under Contract DAAL03-89-C-0032 with T. Doligalski, J. Harris, and T. Zang as contract monitors.

References

[1]Schlichting, H., *Boundary Layer Theory*, 7th ed., McGraw-Hill, New York, 1979.

[2]Wilcox, D. C., "Alternative to the e^9 Procedure for Predicting Boundary-Layer Transition," *AIAA Journal*, Vol. 19, No. 1, 1981, pp. 56–64.

[3]Wilcox, D. C., "Turbulence-Model Transition Predictions," *AIAA Journal*, Vol. 13, No. 2, 1975, pp. 241–243.

[4]Wilcox, D. C., "Turbulence Model Transition Predictions: Effects of Surface Roughness and Pressure Gradient," AIAA Paper 75-857, June 1975.

[5]Chambers, T. L., and Wilcox, D. C., "Application of the Turbulence-Model Transition-Prediction Method to Flight Test Vehicles," *Turbulence in Internal Flows*, edited by S. N. B. Murthy, Hemisphere, Washington, DC, 1976, pp. 233–247.

[6]Wilcox, D. C., "A Model for Transitional Flows," AIAA Paper 77-126, Jan. 1977.

[7]Wilcox, D. C., and Marvin, J. G., "Combined Effects of Freestream Turbulence and Mass Addition on Blunt-Body Heating and Transition," DCW Industries, Inc., Rept. DCW-R-NC-08, La Cañada, CA, July 1987.

[8]Wilcox, D. C., "Reassessment of the Scale Determining Equation for Advanced Turbulence Models," *AIAA Journal*, Vol. 26, No. 11, 1988, pp. 1299–1310.

[9]Wilcox, D. C., *Turbulence Modeling for CFD*, DCW Industries, Inc., La Cañada, CA, 1993.

[10]Wilcox, D. C., and Traci, R. M., "A Complete Model of Turbulence," AIAA Paper 76-351, July 1976.

[11]Wilcox, D. C., and Rubesin, M. W., "Progress in Turbulence Modeling for Complex Flow Fields Including Effects of Compressibility," NASA TP 1517, April 1980.

[12]Mansour, N. N., Kim, J., and Moin, P., "Reynolds Stress and Dissipation Rate Budgets in Turbulent Channel Flow," *Journal of Fluid Mechanics*, Vol. 194, Sept. 1988, pp. 15–44.

[13]Halleen, R. M., and Johnston, J. P., "The Influence of Rotation on Flow in a Long Rectangular Channel—An Experimental Study," Mechanical Engineering Dept., Stanford University, Stanford, CA, Rept. MD-18, May 1967.

[14]Laufer, J., "The Structure of Turbulence in Fully Developed Pipe Flow," NACA 1174, 1952.

[15]Dryden, H. L., *Aerodynamics and Jet Propulsion*, Vol. V, Princeton Univ. Press, Princeton, NJ, 1959.

[16]Dhawan, S., and Narasimha, R., "Some Properties of Boundary Layer Flow During the Transition from Laminar to Turbulent Motion," *Journal of Fluid Mechanics*, Vol. 3, 1958, pp. 418–436.

[17]Schubauer, G. B., and Skramstad, H. K., "Laminar-Boundary-Layer Oscillations and Transition on a Flat Plate," NACA Rept. 909, 1948.

[18]Fisher, D. F. and Dougherty, N. S., "Transition Measurements on a 10° Cone at Mach Numbers from 0.5 to 2.0," NASA TP-1971, March 1982.

[19]Singer, B. A., Dinavahi, S. P. G., and Iyer, V., "Testing of Transition-Region Models: Test Cases and Data," NASA CR 4371, May 1991.

[20]Schubauer, G. B., and Klebanoff, P. S., "Contributions on the Mechanics of Boundary-Layer Transition," NASA TN 3489, 1955.

[21]Blair, M. F., and Werle, M. J., "Combined Influence of Free-Stream Turbulence and Favorable Pressure Gradients on Boundary Layer Transition and Heat Transfer," United Technologies Rept. R81-914388-17, E. Hartford, CT, March 1981.

[22]Blair, M. F., "Influence of Free-Stream Turbulence on Boundary Layer Heat Transfer and Mean Profile Development, Part 1—Experimental Data," *Transactions of the ASME, Journal of Heat Transfer*, Vol. 105, Feb. 1983, pp. 33–40.

[23]Chen, F.-J., Malik, M. R., and Beckwith, I. E., "Boundary-Layer Transition on a Cone and Flat Plate at Mach 3.5," *AIAA Journal*, Vol. 27, No. 6, 1989, pp. 687–693.